

Chip formation mechanism in dry hard high-speed orthogonal turning of hardened AISI D2 tool steel with different hardness levels

Linhu Tang^{1,2,3} · Jun Yin⁴ · Yongji Sun^{1,2,3} · Hao Shen⁴ · Chengxiu Gao^{1,2,3}

Received: 15 December 2016 / Accepted: 13 June 2017 / Published online: 30 June 2017
© Springer-Verlag London Ltd. 2017

Abstract Serrated chip formed in dry hard turning is considered one of the major chip types. In this paper, the main objective was to understand how the crack initiation and propagation, and thermo-plastic instability and pressure from force contribute to the formation mechanism of serrated chip in dry hard high-speed orthogonal turning (DHHOT) of the hardened steel with different hardness levels at cutting speed with 50, 450, and 850 m/min. The influences of the cutting speeds (50, 450, and 850 m/min) and workpiece hardness (40, 45, 50, 55, and 60 ± 1 Rockwell hardness (HRC)) on chip morphology, segment spacing, degree of segmentation, chip deformation coefficient, shear angle, and chip segmentation frequency also were experimentally investigated. Experimental results showed that the very high strain in the shear band does give rise to the high temperature in higher hardness material and at higher cutting speed and this makes the high-speed slip of the shear band much easier happen along existing micro-crack. The critical chip is produced at a cutting speed of 50 m/min and a hardness level of 50 ± 1 HRC. The strain rate increases with the increments of the cutting speed, which increases brittleness, and thus induces acceleration of the crack propagation

speed in shear band. Moreover, the increments of the quenching hardness can increase the brittleness of the workpiece and thus lead to the large damage in shear band. The microstructure of the material within the bottom of chip showed that the elongated grains do appear due to thermo-mechanical effect between the chip back and the rake face of the cutting tool.

Keywords Serrated chip · Formation mechanism · Crack · Thermo-plastic instability · Hardness · Cutting speed

Nomenclature

v	Cutting speed (meter per minute)
f	Feed (millimeter per revolution)
H	Workpiece hardness (HRC)
b	Chamfer width (millimeter)
α	Rake angle (degrees)
γ_0	Clearance angle (degrees)
F_Y	Radial cutting force (N)
F_Z	Main cutting force (N)

✉ Linhu Tang
tanglinhu@126.com

¹ Provincial Key Laboratory for Green Cutting Technology and Application of Gansu Province (University), Lanzhou Institute of Technology, Lanzhou, People's Republic of China

² College of Mechano-Electronic, Lanzhou Institute of Technology, Lanzhou, People's Republic of China

³ Present address: No. 1 Gongjiaping East Road, Lanzhou 730050, Gansu Province, People's Republic of China

⁴ College of Mechano-Electronic, Lanzhou University of Technology, Lanzhou 730050, Gansu Province, People's Republic of China

1 Introduction

The dry hard high-speed turning technology is characterized by having brought about many revolutions in manufacturing the molds, cars on account of such its great advantages as improving machining precision, surface quality, drastically shortening machining time, reducing the manufacturing cost, and eliminating environmental pollution resulted from using the cutting fluid compared to grinding [1]. Therefore, this technology should become a most promising machining process of the hardened steels.

However, this technology, so far, has not been widely applied in modern industry. It may be due to the high cutting force, high cutting temperature, and serrated chip as machining high hardness steel ($45\text{--}65 \pm 1$ Rockwell hardness (HRC)), which can give rise to deteriorating the machined surface quality [2] and shorting the tool life.

An extensive work has been studied on the serrated chip formation in dry hard turning because the serrated chip morphology and its formation mechanism are related to the cutting force, cutting temperature, and machined surface integrity. Poulachon and Moisan [3] have considered that it is the cutting speed and workpiece hardness that have influence on the morphology of serrated chip. Then, Joshi, Ramakrishnan, and Ramakrishnan [4] have found that a fracture initiates on the free surface of the chip, and then it propagates toward the cutting tool nose. They have thought that the cutting speed has important influence on the fracture propagation. Furthermore, Guo, Yen, and David [5] have investigated the discontinuous chip in high-speed machining hardened steel AISI4340 with 32 HRC hardness. In their paper, the formation propagation of workpiece crack is simulated by using the Johnson-Cook model. Dolinšek, Ekinović, and Kopač [6] have considered that there is a relationship among these chip parameters by experimentally studying the segmentation frequency and chip shape, as well as chip formation mechanism in conventional and high-speed (50–1500 m/min) machining of the hardened steel X63CrMoV51 (629 HV). Then, an attempt has been made in the literature [7] by predicting the chip formation in orthogonal cutting of hardened steel (AISI 52100, 62 HRC) by using the polycrystalline cubic boron nitride (PCBN) cutting tool. Wan, Wang, and Gao [8] have considered that the temperature softening fails when the cutting speed reaches very high, and the strain rate hardening plays a much more significant role. Later, Zhang and Guo [9] have investigated the influences of the cutting parameters on the chip morphology and phase transformation by using milling of the AISI H13 tool steel with $50 \pm$ HRC. The microstructure analysis showed that serrated chip and white layer are produced only under a certain condition of the feed and high cutting speed. In addition, the influences of material brittleness on serrated chip formation and morphology were studied by Su and Liu [10]. The results showed that the material brittleness heavily influences the chip morphology. Besides Mhamdi, Ben Salem, Boujelbene, etc. [11], who have studied the mechanism of chip formation in dry hard turning of hardened steel EN X160CrMoV12 (62 ± 1 HRC), Sutter and List [12] have considered that the cutting speed has the most important influence on the chip formation, shear angles, frequency of segmentation, and the crack length compared with the uncut chip thickness.

The damage evolution mechanisms of adiabatic shear localized fracture in chip formation have been investigated in high-speed machining of the hardened AISI 1045 steel

($50 \pm$ HRC) at the cutting speeds ranging from 100 to 1400 m/min [13]. They have thought thermal softening effect plays a key role in the process of adiabatic shear localized fracture. Moreover, Wang, Xie, Zheng, et al. [14] have investigated the chip formation and the chip morphology, as well as formation condition of continuous and serrated chip in high-speed milling of hardened steel with 51 and 62 HRC hardness. However, workpiece has merely been hardened to the only two hardness levels with 51 and 62 ± 1 HRC. Zhang, Shivpuri, and Srivastava [15] have considered that the crack does propagate to the chip-free surface when tool advances. Furthermore, Nakayama, Arai, and Kanda [16] have considered that the crack initiates at the chip-free surface when the strain in the chip exceeds the material limiting strain during the formation of serrated chip. Yang and Li [17] investigated the formation mechanism of the chip in high-speed machining of the alloy cast iron. The results show that the serrated chip is caused by the thermoplastic instability and plastic instability.

The deformation mechanism of chip analysis involved in the chip formation process as well as the conditions is an effective way by utilizing to proper and even deeper study understanding of machining process. It can be indicated from above literatures that there are few researches focusing on the formation mechanism of serrated chip in conventional and high-speed dry hard turning of the hardened tool steel AISI D2 with different hardness levels ranging from 40 to 60 ± 1 HRC.

In this paper, the main purpose of the study is to investigate the influence of the cutting speed and hardness level on the chip formation process. And what is more, the chip formation mechanism and the transition mechanism from continuous to serrated chip are obtained in dry hard high-speed orthogonal turning of hardened AISI D2 tool steel with different hardness levels. Also, the segment spacing, chip segmentation frequency, degree of segmentation, chip deformation, shear angle, and cracking frequency are all discussed in this paper.

2 Experimental procedures

2.1 Workpiece material

The workpiece material used in this experiment was a AISI D2 tool steel (Cr12MoV, China) bar with chemical composition shown in Table 1.

Table 1 Chemical composition of the AISI D2 tool steel (wt%)

C	Cr	Mo	Mn	Si	P	S	V
1.55	11.25	0.45	0.35	0.35	0.025	0.025	0.20

2.2 Heat treatment workpiece

The results in the literature [18] showed that the this marerial may get much higher hardness and better mechanical properties if quenching in the temperatures from 1000 to 1040 °C. The heat treatments were carried out by using the methods in the literature [19].

Figure 1a–e presents the microstructure micrographs of the hardened steel AISI D2 with 40 ± 1 , 45 ± 1 , 50 ± 1 , 55 ± 1 , and 60 ± 1 HRC hardness levels, respectively.

2.3 Workpiece

The cylindrical workpiece was specifically designed. It has a diameter of 128 mm and length of 210 mm, as shown in Fig. 2a.

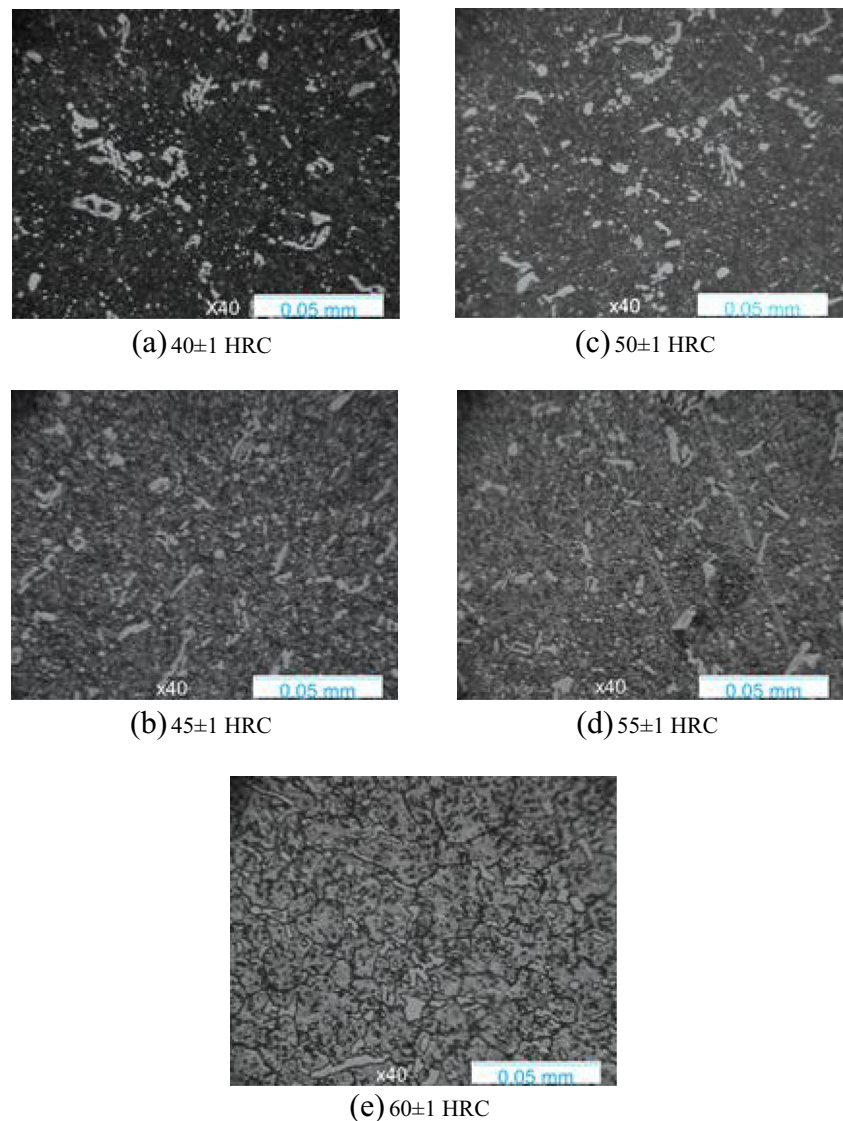
2.4 Hardness measurement

Measurement of hardness was carried out by digital Rockwell hardness tester (type: HRS-150). Then, the hardened workpieces were classified and chosen according to the experimental demand. At last, the workpieces with 40 ± 1 , 45 ± 1 , 50 ± 1 , 55 ± 1 , and 60 ± 1 HRC hardness levels were obtained.

2.5 Microstructure and measurement of the serrated chip sample

The chip samples collected in DHHOT of hardened steel were vertically set into the mixture of epoxy resin. Then, the samples were polished by utilizing a grinding-polishing machine. Figure 3 shows the finished specimens.

Fig. 1 Microstructure of the workpiece with different hardness levels



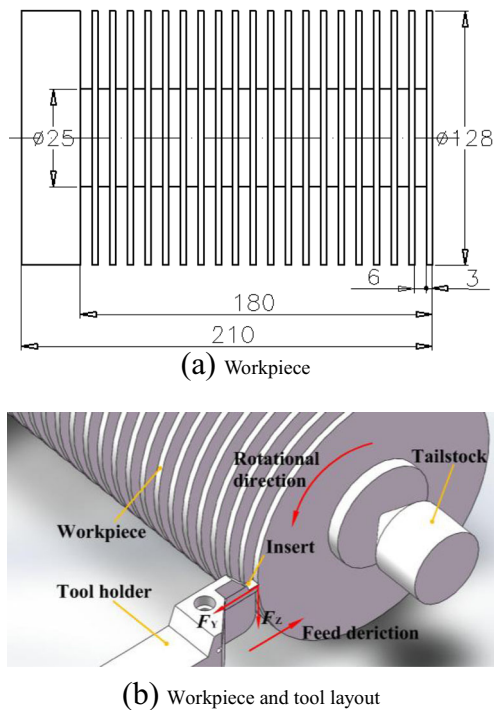


Fig. 2 Scheme for orthogonal hard turning tests

Metallographic samples were obtained by etching in 4% nitric acid alcohol solution between 30 and 120 s. The observation of the micro-morphology and measurement of serrated chip were conducted by using a digital metallurgical microscope (type: HXD-1000TMJC/ LCD). As can be seen in Fig. 4, the serrated chip sizes are described in serrated chip thickness h_1 , chip thickness at local shear deformation h_2 , shear angle Φ , serrated chip angle Φ_1 , and distance of serrated chip segmentation p_c .

The chip samples were also examined by using an INSPECT F50 scanning electron microscope (SEM).

2.6 PCBN cutting tool

In this paper, the PCBN inserts (type: BZNHTM 2100, DI) containing the CBN with 2- μm grain size and 50% CBN composition by volume were chosen according to



Fig. 3 Finished specimens

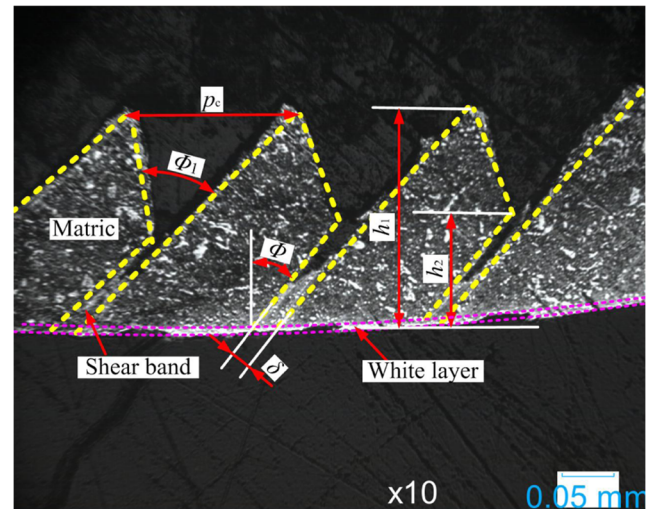


Fig. 4 Chip morphology and measurement of a serrated chip when orthogonal cutting workpiece with 45 HRC hardness

the literature [20] in DHHOT of the hardened tool steel. In DHHOT, the carbide and CBN can, respectively, provide shock resistance and very high wear resistance. The composite PCBN inserts with 5-mm cutting edge length and 0.1-mm chamfer width made in Beijing World Company were utilized in DHHOT of the hardened tool steel, as presented in Fig. 5. As shown in Fig. 2b, it was mounted on a cutter holder resulting in a rake of 5° , clearance angles of 7° .

2.7 DHHOT tests

As described in Fig. 6, the Kistler dynamometer (type: 9257C) and thermal infrared imager (type: DM63-II) mounted on a lathe (type: CAK5085si) with the power of 7.5 kW and speeds ranging from 22 to 2500 rpm was employed. The main cutting force F_z , radial cutting force F_y , and cutting temperature were measured by the Kistler dynamometer and the thermal infrared imager.

Experiments have been carried out over different cutting speeds of 50, 450, and 850 m/min and a fixed feed of 0.20 mm.

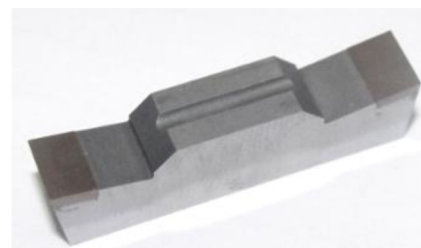
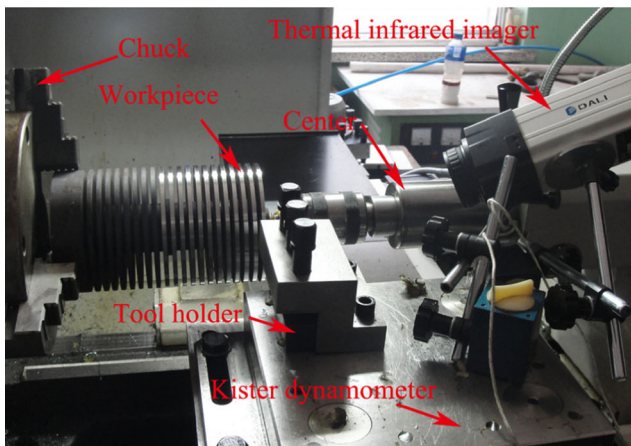


Fig. 5 PCBN insert



(a) DHHOT test system



(b) Photograph of the partial enlargement

Fig. 6 Experimental setup employed during the DHHOT tests

3 Results

3.1 Chip morphology

Tables 2, 3, and 4 present the influences of the hardness levels on the chip morphology in three cases of 50, 450, and 850 m/min cutting speeds. It can be seen in Table 2 that chip macrographs are the spring chip, tight helix chip, tower chip, spring chip, and incompact helix chip with increments of the hardness levels. Yet, the continuous ribbon chip begins to transform into the continuous serrated chip due to occurrence of shear slip in primary deformation zone when the workpiece hardness reaches 50 HRC in a case of 50 m/min cutting speed.

However, as shown in Table 3, the tightly curled chip called tight helix chip only does occur in DHHOT of the workpiece with 50 ± 1 HRC hardness. It is interesting that the “C” type chip appears in the case of a 45 ± 1 HRC. Note the continuous serrated chip happens in DHHOT of the five hardness level workpieces at a cutting speed of 450 m/min, which differs from the lower cutting speed of 50 m/min.

As can be seen explicitly in Table 4, the tightly curled helix chips occur in the cases of 40 and 50 ± 1 HRC hardness levels at a 850 m/min cutting speed, and tower chip happens only in the case of a 45 ± 1 HRC hardness level. The section of chip indicates that serrated chips appear.

3.2 Segment spacing

Figure 7 describes the variation of the segment spacing with the hardness at three cutting speeds of 50, 450, and 850 m/min. It can be observed from this figure that the cutting speed and quenching hardness have the significant influence on the segment spacing. In the cases of 40 and 45 ± 1 HRC hardness levels, the segment spacing is zero at a 50 m/min cutting speed shown in Table 2, while it gradually increases with increments of the cutting speed. However, there is a more complex changing law for the segment spacing at 450 m/min compared to the cutting speeds of 50 and 850 m/min. In addition, it is obvious that the segment spacing gradually decreases in the wavy way. The segment spacing gradually increases with increments of the hardness and attains the peak value in the case of a 55 ± 1 HRC and then a sudden drop does occur in the case of a 60 HRC at 850 m/min.

3.3 Degree of segmentation

Here, the degree of segmentation can be generally described as follows [21]:

$$G_s = (h_1 - h_2) / h_1 \tag{1}$$

As can be seen in Fig. 8, the degree of segmentation gradually increases with increments of the hardness at 50, 450, and 850 m/min cutting speeds. Clear visible result is that the degree of segmentation is more significant at the cutting speeds of 450 and 850 m/min than that at 50 m/min. It shows that the workpiece hardness and cutting speed have important influence on the degree of segmentation.

3.4 Chip deformation coefficient

The deformation coefficient ξ of the continuous chip is that the ratio of the chip thickness h_{ch} to the depth of cut h_D (here is the feed), as expressed in Eq. (2).

$$\xi = \frac{h_{ch}}{h_D} \tag{2}$$

The deformation coefficient ξ of the serrated chip can be obtained by using Eq. (3).

$$\xi = \frac{h_2 + (h_1 - h_2) / 2}{h_D} \tag{3}$$

Table 2 Morphology of chip in DHHOT of workpiece with different hardness levels in a case of 50 m/min cutting speed


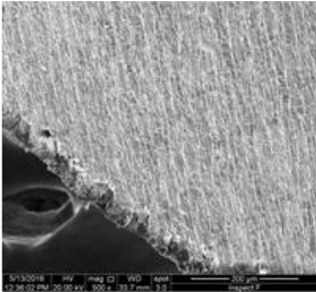
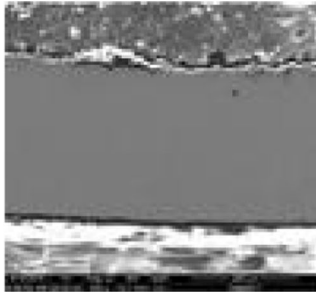


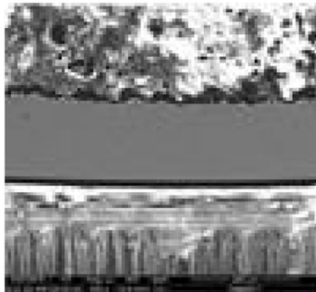

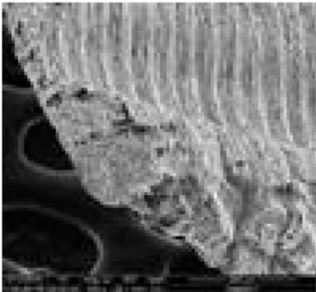
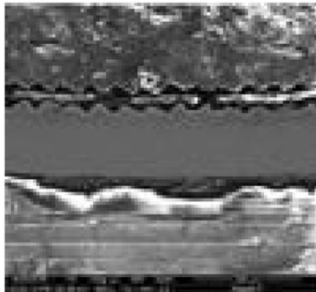

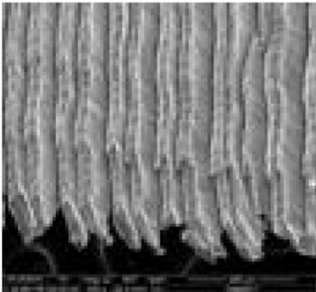
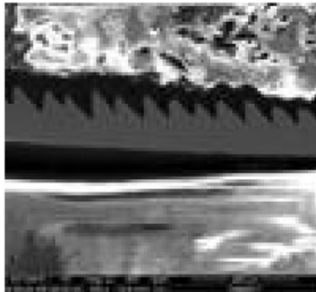

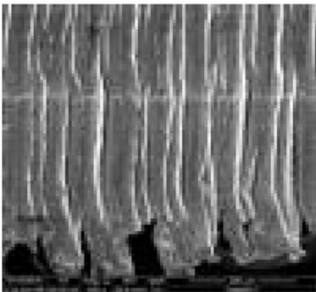
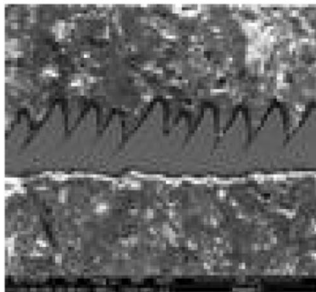
Quenching hardness (±1 HRC)	Morphology of chip		
	Macrograph of chip	Micrographs of chip (SEM)	Section of chip (SEM)
40			
45			
50			
55			
60			

Table 3 Morphology of chip in DHHOT of workpiece with different hardness levels in a case of 450 m/min cutting speed


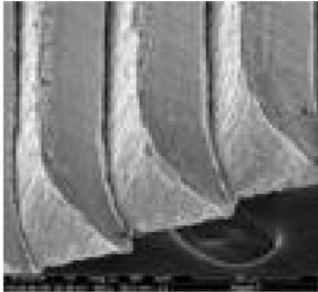
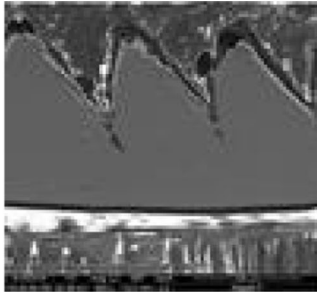


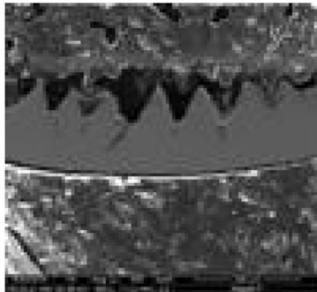

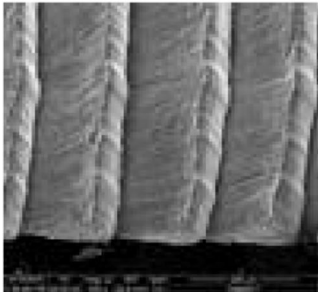
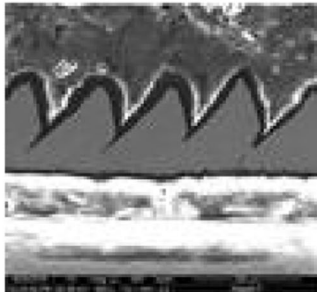

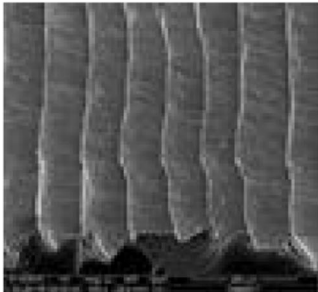
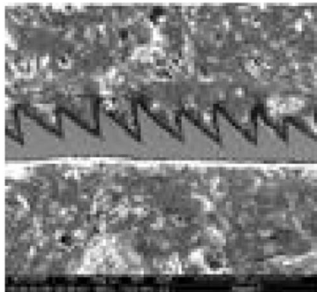

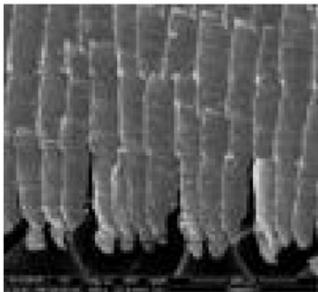
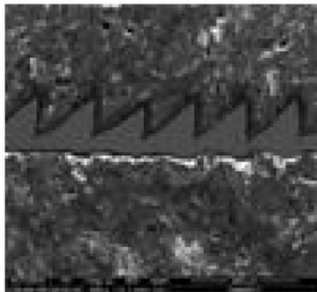

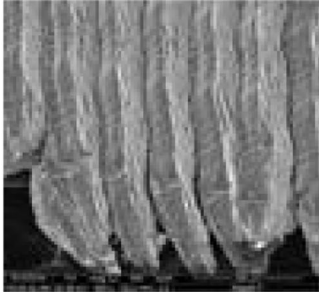
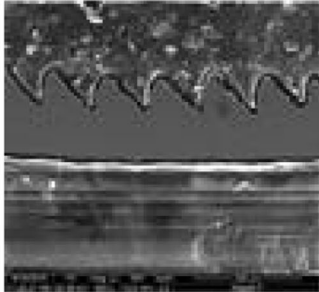

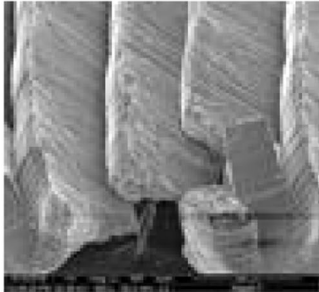
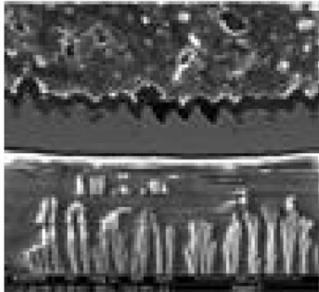

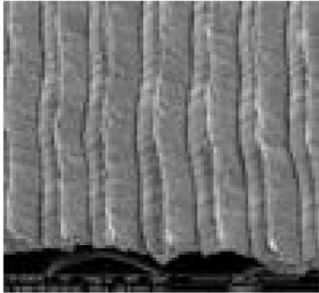
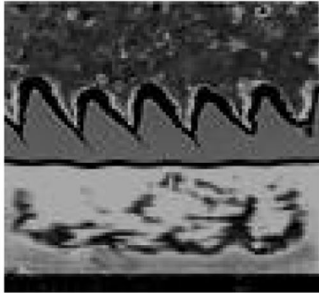

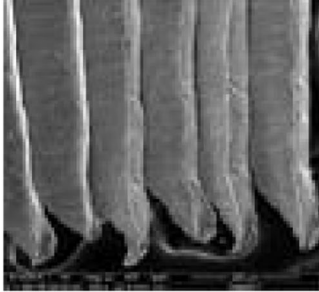
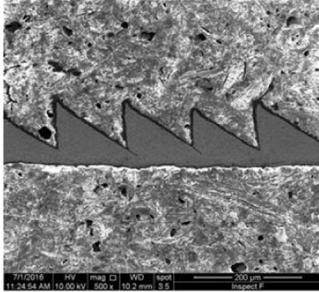

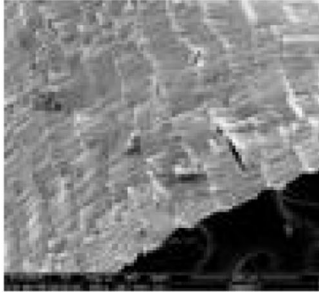
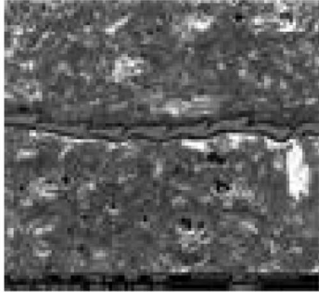
Quenching hardness (±1 HRC)	Morphology of chip		
	Macrograph of chip	Micrographs of chip	Section of chip
40			
45			
50			
55			
60			

Table 4 Morphology of chip in DHHOT of workpiece with different hardness levels in a case of 850 m/min cutting speed

Quenching hardness (±1 HRC)	Morphology of chip		
	Macrograph of chip	Micrographs of chip	Section of chip
40			
45			
50			
55			
60			

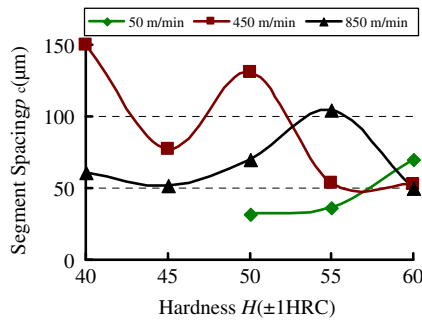


Fig. 7 Segment spacing of sawtooth chip at a fixed feed of 0.20 mm/r

It can be observed in Fig. 9 that the deformation coefficient sharply drops as the workpiece range from 40 to 45 ± 1 HRC in the cases of 50, 450, and 850 m/min. In the range from 45 to 60 ± 1 HRC hardness levels, it varies in different ways. A gradual decline continues in a case of 50 m/min cutting speed, while it slowly increases and attains the highest peak in a case of 450 m/min, then gradually decreases with increments of the workpiece hardness, as shown explicitly in Fig. 9. In addition, the similar variation in a case of 850 m/min does occur. The only difference is that the peak value appears at a hardness of 55 ± 1 HRC.

3.5 Shear angle

Figure 10 shows that there are similar changing laws for the shear angle in the cases of 450 and 850 m/min in the range from 40 to 50 ± 1 HRC hardness. They slowly decrease and then increase considerably as the workpiece hardness increases. However, it begins to gradually decrease at a cutting speed of 850 m/min, while continuous increase occurs as the cutting speed reaches 450 m/min.

3.6 Chip segmentation frequency

The chip segmentation frequency of the serrated chip can be obtained by using Eq. (4).

$$CF = \frac{v \sin \phi}{p_c \cos(\phi - \alpha)} \tag{4}$$

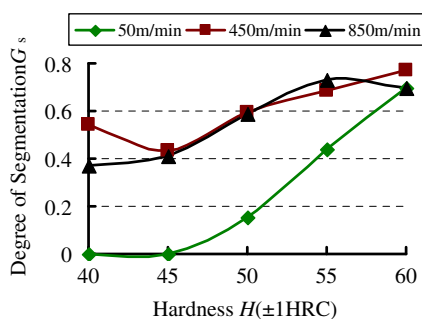


Fig. 8 Degree of segmentation at a fixed feed of 0.20 mm/r

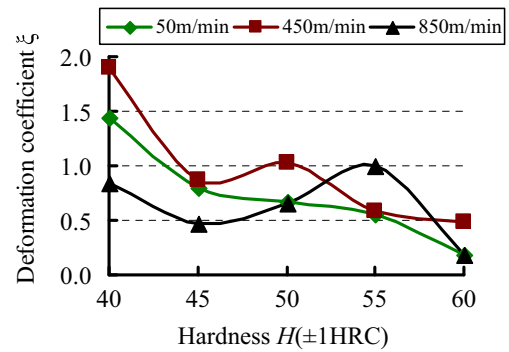


Fig. 9 Chip deformation coefficient at a fixed feed of 0.20 mm/r

As can be seen in Fig. 11, the chip segmentation frequency decreases slightly with increments of the hardness varying from 50 to 60 ± 1 HRC at a 50 m/min cutting speed. It is clearly observed from this figure that the changing law at a cutting speed of 450 m/min is similar to that at 850 m/min when the hardness ranges from 40 to 50 ± 1 HRC, while it has distinctly different changing law at 50 and 60 ± 1 HRC hardness. It firstly suddenly rises for a 50 ± 1 HRC hardness and then gradually increases for a 55 ± 1 HRC hardness at 450 m/min, while it abruptly drops in the range from 45 to 55 ± 1 HRC hardness and then suddenly increases for a 60 ± 1 HRC at 850 m/min. Besides, it is much higher at higher cutting speeds in comparison with that at the lower cutting speeds, which is in agreement with the literature [22].

4 Discuss

4.1 Formation mechanism of the serrated chip

Figures 12, 13, and 14 present the microstructures of chips in DHOT of the hardened AISI D2 steel with different hardness levels from 45 to 60 ± 1 HRC at 50, 450, and 850 m/min cutting speeds and 0.2 mm/r feed.

It can be seen in Fig. 12a–c that the ribbon chip does occur when the hardness varies from 40 to 50 ± 1 HRC hardness, and not only the crack but the localized shear deformation does not occur. The shear deformation does happen and the

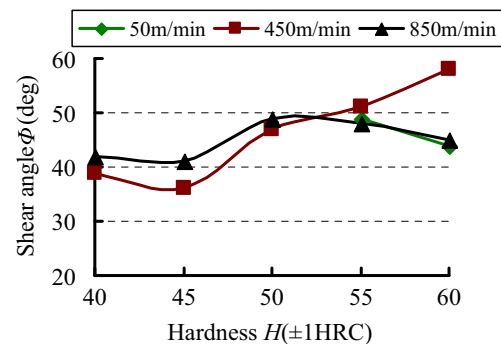


Fig. 10 Shear angle at a fixed feed of 0.20 mm/r

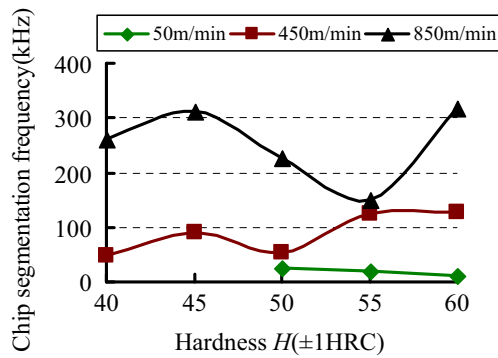
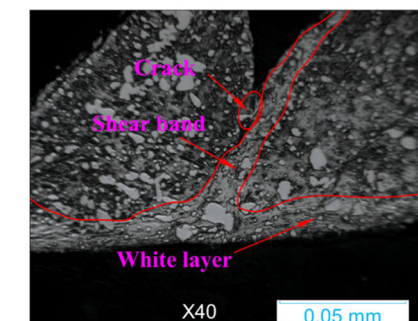
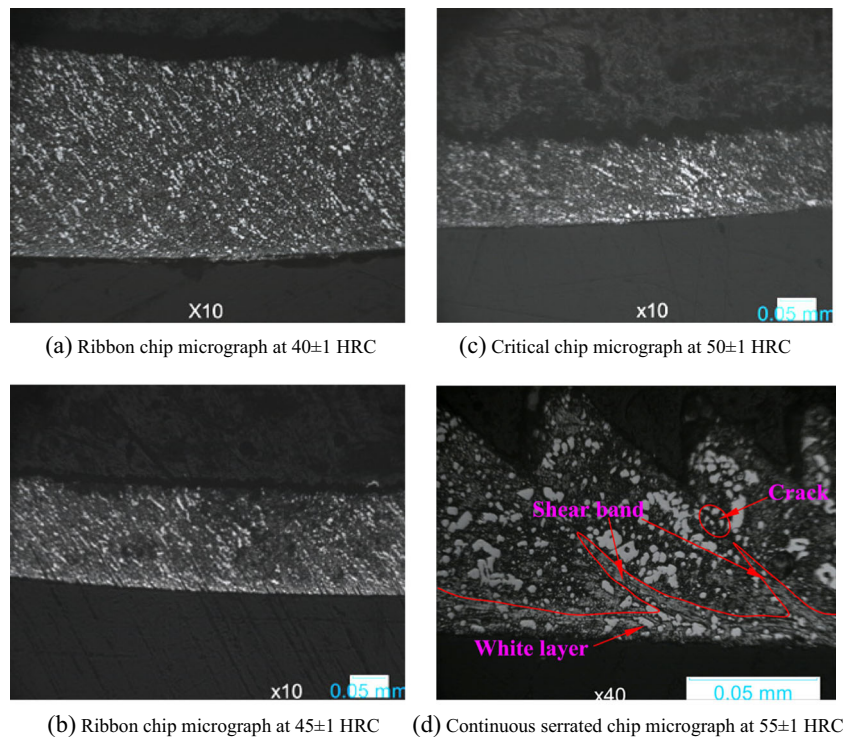


Fig. 11 Chip segmentation frequency at a fixed feed of 0.20 mm/r

serrated chip begins to appear in Fig. 12d, e in DHHOT of the two hardness levels of 55 and 60 ± 1 HRC. It can be seen also in Fig. 12e that the adiabatic shear band that originated within a localized region does propagate to the free surface in the case

Fig. 12 Chip micrograph of hardened AISI D2 steel at a cutting speed of 50 m/min

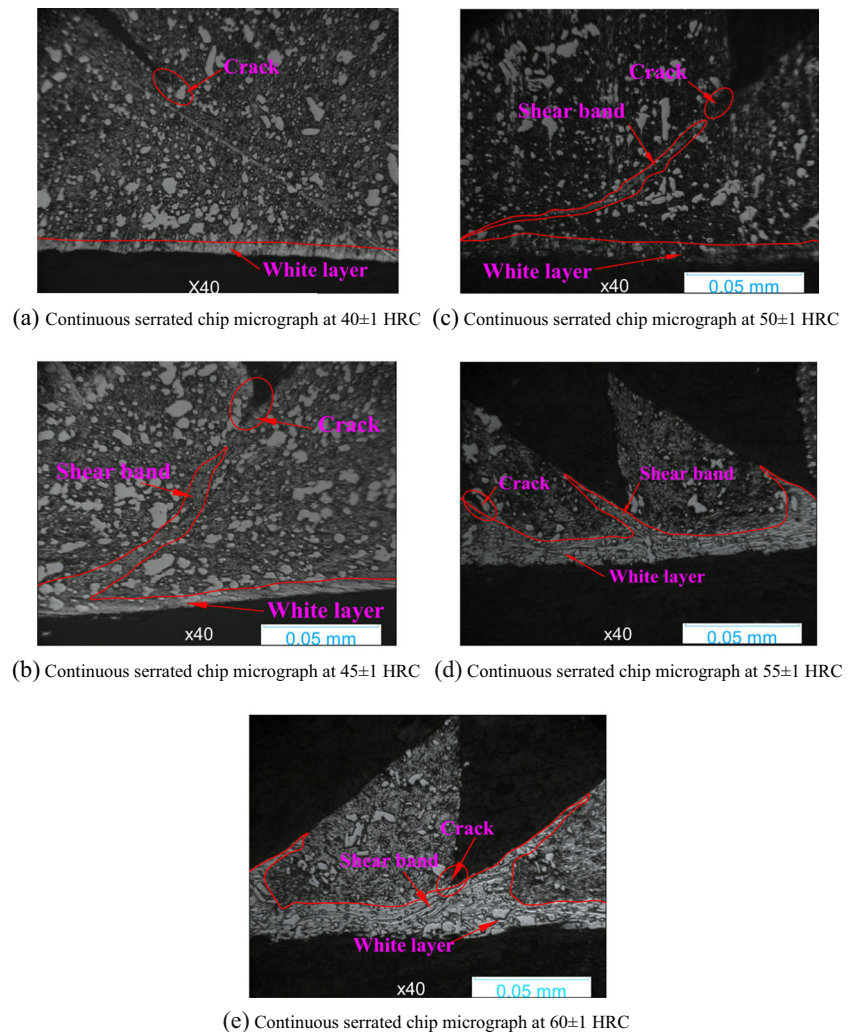


(e) Continuous serrated chip micrograph at 60±1-HRC

of a 60 ± 1 HRC, while it does not happen at 55 ± 1 HRC. In addition, it can be observed in Fig. 12d, e that the crack periodically initiates on the free surface and propagates due to the promotion resulted from the compressive hydrostatic stress in shear band direction, which is in agreement with the literature [23]. It can be shown from above experimental evidences that it is the adiabatic shear and crack that induces serrated chip formation in DHHOT of the hardened AISI D2 steel with 55 and 60 ± 1 HRC hardness levels.

Further increasing the cutting speed to 450 m/min, no ribbon chip does occur, while serrated chip appears and the degree of segmentation increases with increments of the quenching hardness, as shown in Figs. 8 and 13a–e. Furthermore, the localized shear band becomes much clearer with increments of the quenching hardness. Instead of the localized shear band, a distinct crack along the shear plane is observed in a case of 40 ± 1 HRC hardness at a cutting speed of 450 m/min, as shown in Fig. 13a.

Fig. 13 Chip micrograph of hardened AISI D2 steel at a cutting speed of 450 m/min



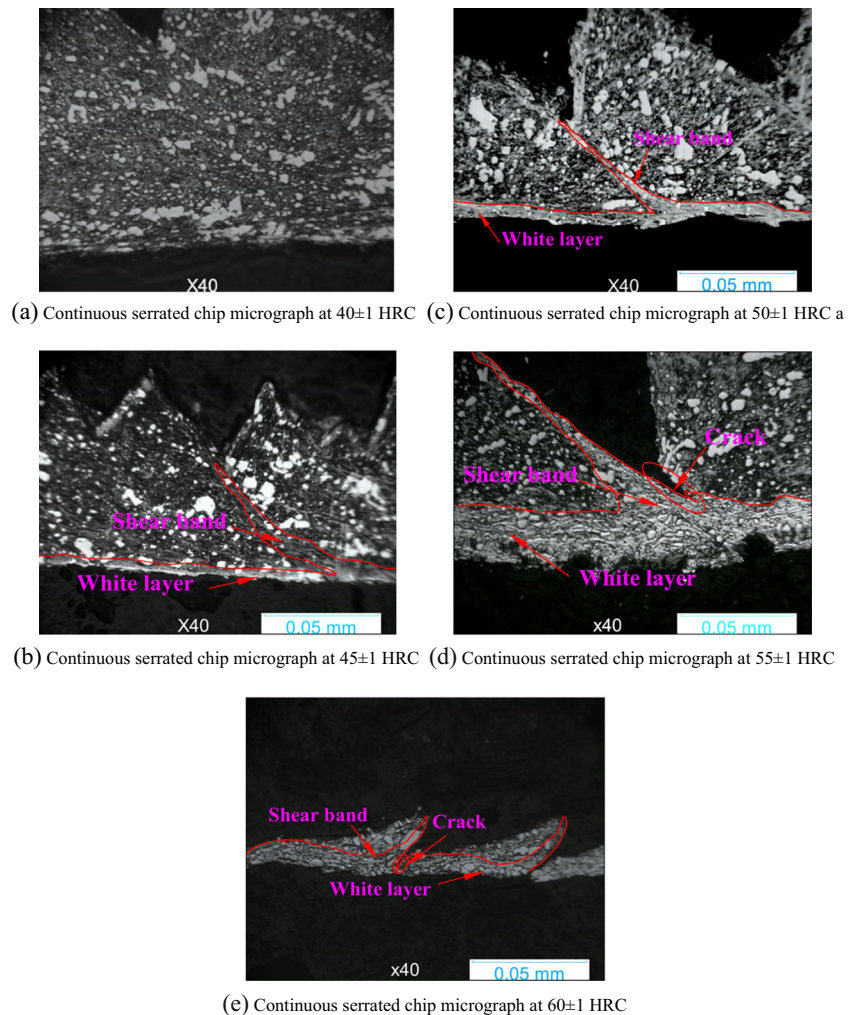
The adiabatic shear band does propagate to the free surface at the hardness levels of 55 and 60 ± 1 HRC, as shown in Fig. 13d, e, while it does not occur at 45 and 50 ± 1 HRC. In addition, the crack on the free surface can be observed in all of the five hardness levels. The microstructure of the material within the back of chip shows that the elongated grains do appear owing to the friction between the chip back and the rake face of the cutting tool as the hardness reaches to 55 and 60 ± 1 HRC, as presented in Fig. 13d, e. Furthermore, it is clearly visible that the white layer within the chip bottom does occur, which is a consequence of the effect of thermo-mechanical effect.

It can be seen in Fig. 14a–e that when the cutting speed further increases to 850 m/min, the localized shear band becomes more obvious and it begins to occur at a lower hardness of 45 ± 1 HRC compared to the cutting speeds of 50 and 450 m/min, shown in Fig. 14b. The reasons can be attributed to the below further reasons: when high-speed cutting, the generated temperature in localized shear band cannot flow into the chip in a very short time, which induces the rate of

heat generation much more than the rate of heat dissipation, and thus the material in localized shear band becomes softer than those in the cutting speeds of 50 and 450 m/min. Additionally, the serrated chip thickness h_1 in turning of workpiece with 60 ± 1 HRC hardness is even with thinner thickness in comparison to those of the other four lower hardness levels.

Based on the examinations in Figs. 12, 13, 14, and 17, the width of shear band varies along the primary zone, and comparing with the width of shear band nearer the free surface, it is far thicker in the vicinity of the serrated chip bottom where, in general, the shear band initiates. This supports the thermo-plastic shear theory of serrated chip formation [24]. Obviously, the very high strain in the shear band does give rise to the high temperature in higher workpiece hardness and higher cutting speeds, which make the high-speed slip of the shear band much easier to happen along existing micro-crack. The crack continues to propagate until it stops at the limit of the material plastic deformation zone. In general, this phenomenon is promoted by the high heat generated in the cutting zone, which is in good agreement with literature [25]. The fact

Fig. 14 Chip micrograph of hardened AISI D2 steel at a cutting speed of 850 m/min



is that workpiece hardness is very important in further urging the crack initiation.

The adiabatic shear band that originates within a localized region also does propagate to the free surface as high-speed turning of workpiece with the hardness from 45 to 60 ± 1 HRC, as observed in Fig. 12b–e. Meanwhile, the crack occurs

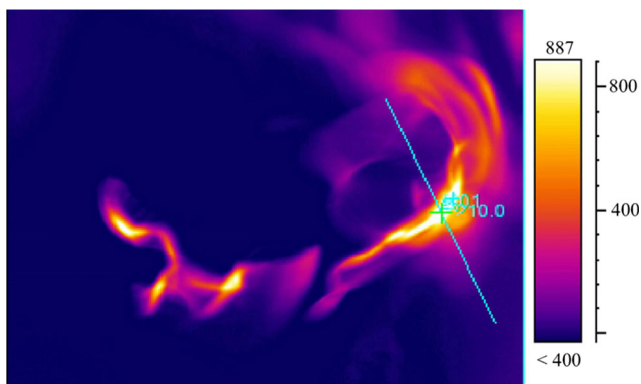


Fig. 15 Temperature field of chip in a case of 60 ± 1 HRC at the cutting speed of 850 m/min

only in the cases of 40, 55, and 60 ± 1 HRC. Figure 14b–e shows that the white layer within the chip bottom is more obvious and much wider compared to those at 50 and 450 m/min.

Note the serrated chip size h_1 in a case of 60 ± 1 HRC hardness at a cutting speed of 850 m/min is much thinner relative to lower cutting speeds. Figure 15 presents that the temperature field of chip is conducted by the thermal infrared imager in case of 60 ± 1 HRC at 850 m/min. As shown in the figure, the temperature reached the height of over 887 °C, which indicates the high heat generation occurs, and it is absorbed sufficiently by chip flying away the rake face of the cutting tool, and thus these heat soften the chip, together with the pulling force, and the serrated chip size h_1 grows thin.

Figure 15 also presents that the temperatures in shear band should reach a phase transformation value of above 900 °C as turning of the hardness from 55 to 60 ± 1 HRC at a cutting speed of 50 m/min, from 50 to 60 ± 1 HRC at 450 m/min, and from 45 to 60 ± 1 HRC at 850 m/min, as shown in Figs. 12d, e, 13c–e, and 14b–e. These white areas have been identified as fine un-tempered martensite, which indicates that serrated

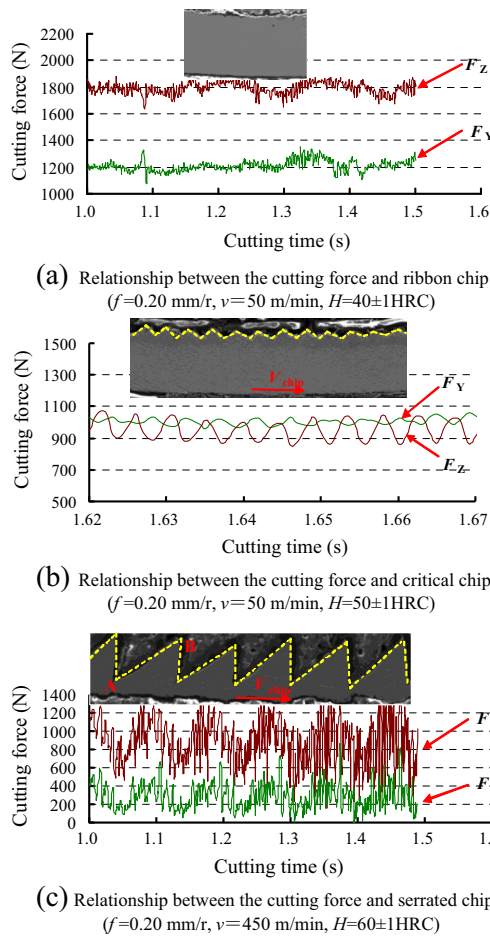


Fig. 16 Relationship between the cutting force and chip

chip may be hardened once again when it is cooled rapidly. At the same time, the material in shear band is exposed to a high

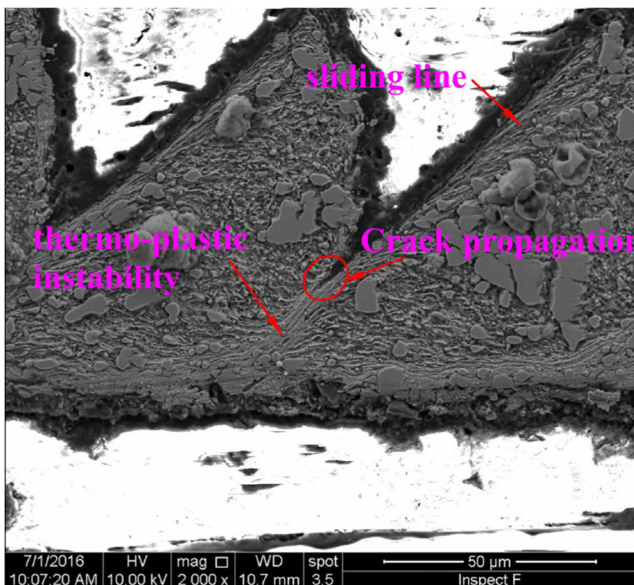
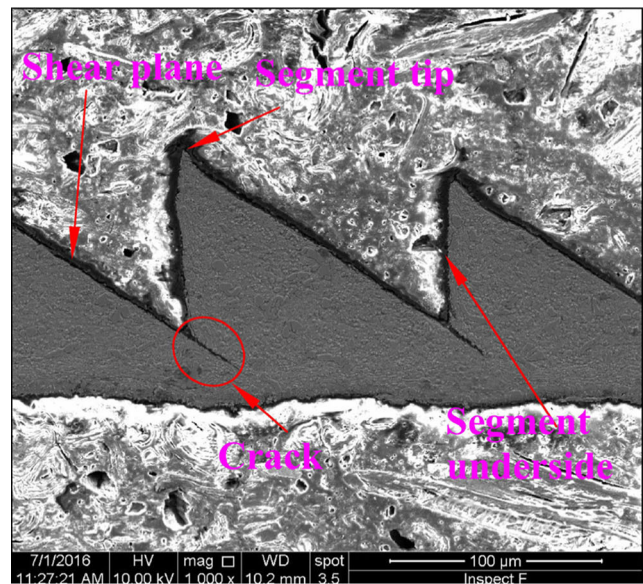
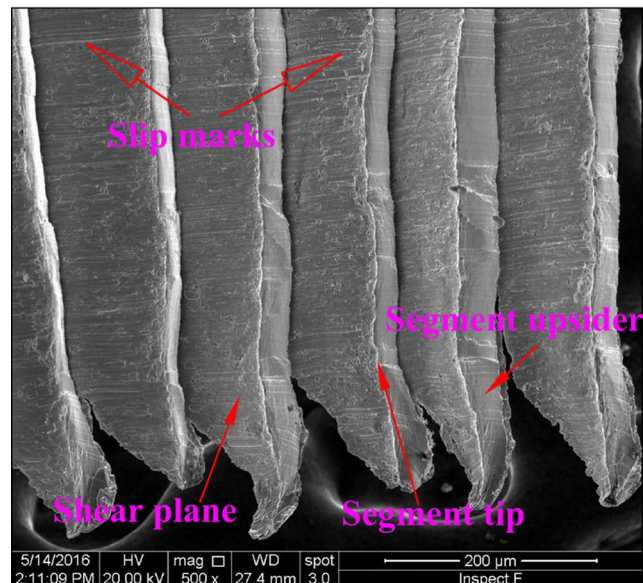


Fig. 17 The crack initiation and propagation and thermo-plastic instability in serrated chip (SEM) ($f = 0.20$ mm/r, $v = 450$ m/min, $H = 60 \pm 1$ HRC)



(a) SEM of section serrated chip micrograph



(b) SEM of free side of serrated chip micrograph

Fig. 18 The SEM of micrographs in DHHOT of hardened steel with 55 ± 1 HRC at the cutting speed of 850 m/min and the feed of 0.2 mm

compressive stress. It should be noted that the hardened tool steel AISI D2 is more inclined to the adiabatic shear theory with increments of the cutting speed and the hardness levels owing to its low thermal conductivity and specific heat, which is similar to the literature [26].

4.2 The cutting force contribution to the formation mechanism of serrated chip

The relationship between the cutting force and chip is analyzed in Fig. 16a–c in order to study the formation mechanism of the serrated chip. It is interesting that the main cutting force

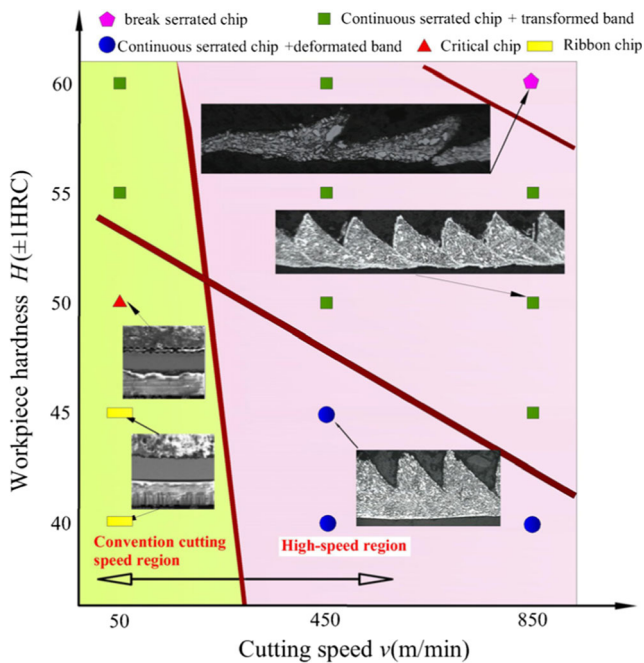


Fig. 19 The critical cutting conditions of continuous serrated chip and isolated chip

F_Z and radial cutting force F_Y do decrease with the transition from ribbon chip to serrated chip. It can be seen in Fig. 16a that the ribbon chip is produced in the steady cutting process and the mean value of the main cutting force F_Z is much higher comparing with the radial cutting force F_Y . In addition, the main cutting force F_Z is characterized by the quasi-dynamic cutting as the critical chip appears and the main cutting force F_Z and radial cutting force F_Y are approximately equal, as shown in Fig. 16b. However, note that only the main

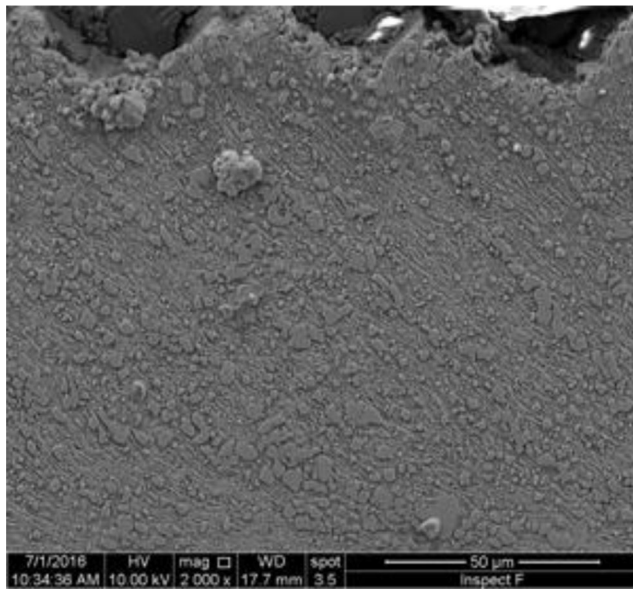


Fig. 20 The critical chip in transition between ribbon chip and serrated chip (SEM) ($f = 0.20$ mm/r, $v = 50$ m/min, $H = 50 \pm 1$ HRC)

cutting force F_Z presents larger vibration related to the radial cutting force F_Y .

As can be observed in Fig. 16c, the cyclic main cutting force F_Z and radial cutting force F_Y present dynamic change according to the change law of the serrated chip, which shows the segmented chips do generate the cyclic dynamic load on the cutting tool and the cutting force frequency is very similar to the chip segmentation frequency. This reason contributes to the two mechanisms: crack and thermo-plastic instability. On one hand, obviously, the cutting pressure imposed in the advancing direction of the cutting tool should be considered resulting in the crack initiation decreasing the cutting force. On the other hand, the critical thermo-plastic instability at the initial stage of turning does occur owing to heat soften effect [11] in the shear band, which contributes to the decrease of flow stress and thus the main and radial cutting forces abruptly decrease. After this, the sliding along dashed line occurs and even extends from the cutting tool tip to the free surface promoted by the crack initiation and propagation, thermo-plastic instability, and the cutting pressure imposed in the advancing direction of cutting tool, and thus, the root A and tip B of the serrated chip form, as shown in Figs. 16 and 17.

Figure 18a, b presents a section optical and SEM micrograph of a serrated chip in a case of 60 ± 1 HRC hardness at a cutting speed of 850 m/min. Obviously, the shear plane on each serrated chip segment is characterized by the presence of parallel slip marks resulted from the thermo-plastic instability and pressure from the cutting tool rake face.

4.3 Critical condition and transformation mechanism from the ribbon chip to serrated chip

It can be observed in Table 2 that the lamellar chips that appear with relatively constant thickness appear in cases of hardness with 40 and 45 ± 1 HRC at 50 m/min, while a new structure termed folds on the free surface of a ribbon chip in a case of hardness with 50 ± 1 HRC does occur. Further increasing the hardness level and cutting speed, the transition from the lamellar ribbon chip to the folded ribbon chip and then to the serrated chip occurs. The chip surface temperatures measured by the thermal infrared imager in cases of 40, 45, and 50 ± 1 HRC at a cutting speed of 50 m/min are 522, 530, and 621 °C, respectively. This reveals that there is a relationship between the transition of chip and the thermal-softening effect in the shear band.

Figure 19 illustrates the influence of the cutting speed and quenching hardness on the transition from ribbon chip to serrated chip. The cutting speed has a significant influence on the serrated chip formation. The higher the cutting speeds are, the easier the formation of the serrated chips are, and the lower the quenching hardness of forming the serrated chip is. It indicates that the strain rate heightens with the increments of the cutting speed, which increase brittleness, and thus induces the

accelerating crack propagation speed in shear band. Moreover, the increments of the quenching hardness can increase the brittleness of the workpiece and thus lead to the large damage in shear band. As a result, it is both the cutting speed and quenching hardness that are the crucial factors promoting the shear band formation.

The critical chip may be defined as the chips in transition between the ribbon chip and serrated chip formation. In this experiment, the critical condition of forming the critical chip is the cutting speed of 50 m/min and hardness level of 50 ± 1 HRC. As shown in Fig. 20 of the critical chip, there is evidence of some upward rise, but no evidence of crack initiation. Moreover, the interesting shear band does occur, yet the slip distance of shear band is very short. The transformed band has begun to form in three cases of 55 ± 1 HRC hardness level and 50 m/min cutting speed; 50 ± 1 HRC hardness level and 450 m/min cutting speed; and 45 ± 1 HRC hardness level and 850 m/min cutting speed.

5 Conclusions

In this paper, chip formation mechanism in DHHOT of the hardened AISI D2 tool steel with different hardness levels was investigated. The conclusions are as follows:

- (1) The chip macrographs are the spring chip, tight helix chip, tower chip, spring chip, and incompact helix chip with increments of the hardness levels. The tight helix chip only does occur at a 50 ± 1 HRC. It is interesting that the “C” type chip appears at a 45 ± 1 HRC. The tightly curled helix chips occur at 40 and 50 ± 1 HRC in a case of 850 m/min, and the tower chip only happens at 45 ± 1 HRC.
- (2) The workpiece hardness has the significant influence on the degree of segmentation, chip deformation coefficient, segment spacing, chip segmentation frequency, and shear angle in DHHOT of the hardened steel AISI D2.
- (3) The width of shear band varies along the primary zone, and comparing with the width of shear band nearer the free surface, it is far thicker in the vicinity of the serrated chip bottom where, in general, the shear band initiates. The localized shear bands become clearer with increments of the hardness. The microstructure of the material within the bottom of chip shows that the elongated grains do appear due to thermo-mechanical effect between the chip back and the rake face of the cutting tool.
- (4) The very high strain in the shear band does give rise to the high temperature in higher hardness material and at higher cutting speed, which make the high-speed slip of the shear band happens more along existing micro-crack. The crack continues to propagate until it stops at the ultimate limit of the workpiece material plastic

deformation zone. The hardened tool steel AISI D2 is more inclined to the adiabatic shear theory owing to its low thermal conductivity and specific heat.

- (5) Not only cracks but localized shear deformation do not occur in cases of hardness ranging from 40 to 60 ± 1 HRC at 50 m/min cutting speed. The localized shear deformation does happen and the serrated chip appears in cases of 55 and 60 ± 1 HRC. The adiabatic shear band that originated within a localized region does propagate to the free surface in a case of 60 ± 1 HRC hardness, while it does not happen at a 55 ± 1 HRC.
- (6) The reasons generating high dynamic load on the cutting tool contribute to the two mechanisms of crack and thermo-plastic instability. The sliding along the shear band occurs extending from the cutting tool tip to the free surface helped by the crack initiation and propagation, thermo-plastic instability, and the cutting pressure imposed in the advancing direction of cutting tool.
- (7) The brittleness induced by promoting the cutting speed and quenching hardness leads to large damage in shear band. The critical chip does occur in a case of 50 ± 1 HRC hardness at a 50 m/min cutting speed.

Acknowledgments This project is supported by the National Natural Science Foundation of China (Grant No. 51465028) and the Youth Innovative Talents Support Plan of Longyuan.

References

1. Tang L, Gao C, Huang J, Shen H, Lin X (2006) Experimental investigation of surface integrity in finish dry hard turning of hardened tool steel at different hardness levels. *J Adv Manuf Technol* 77(9–12):1655–1669
2. Wan L, Wang DZ, Gao YY (2016) The investigation of mechanism of serrated chip formation under different cutting speeds. *J Adv Manuf Technol* 82(5–8):1655–1669
3. Poulachon AL, Moisan J (2000) Hard turning: chip formation mechanisms and metallurgical aspects. *J Manuf Sci E-T ASME* 122(3):406–412
4. Joshi SS, Ramakrishnan N, Ramakrishnan P (2001) Microstructural analysis of chip formation during orthogonal machining of Al/SiCp composites. *J Eng Mater Technol* 123(3):315–321
5. Guo YB, Yen DW (2004) A FEM study on mechanisms of discontinuous chip formation in hard machining. *J Mater Process Technol* 155–156:1350–1356
6. Dolinšek S, Ekinović S, Kopač J (2004) A contribution to the understanding of chip formation mechanism in high-speed cutting of hardened steel. *J Mater Process Technol* 157–158:485–490
7. Shi J, Liu CR (2006) On predicting chip morphology and phase transformation in hard machining. *J Adv Manuf Technol* 27(7–8):645–654
8. Wan L, Wang DZ, Gao YY (2009) The investigation of mechanism of serrated chip formation under different cutting speeds. *J Adv Manuf Technol* 82(5–8):951–959
9. Zhang S, Guo YB (2009) An experimental and analytical analysis on chip morphology. Phase transformation, oxidation, and their relationships in finish hard milling. *Int J Mach Tools Manuf* 49(11):805–813

10. Su GS, Liu Z (2010) An experimental study on influences of material brittleness on chip morphology. *J Adv Manuf Technol* 51(1–4):87–92
11. Mhamdi MB, Ben Salem S, Boujelbene M, Bayraktar E (2013) Experimental study of the chip morphology in turning hardened AISI D2 steel. *J Mech Sci Technol* 27(11):3451–3461
12. Sutter G, List G (2013) Very high speed cutting of Ti-6Al-4V titanium alloy—change in morphology and mechanism of chip formation. *Int J Mach Tools Manuf* 66:37–43
13. Gu L, Wang M, Duan C (2013) On adiabatic shear localized fracture during serrated chip evolution in high speed machining of hardened AISI 1045 steel. *Int J Mech Sci* 75:288–298
14. Wang C, Xie Y, Zheng L, Qin Z, Tang D, Song Y (2014) Research on the chip formation mechanism during the high-speed milling of hardened steel. *Int J Mach Tools Manuf* 79:31–48
15. Zhang X, Shivpuri R, Srivastava AK (2016) Chip fracture behavior in the high speed machining of titanium alloys. *J Manuf Sci E-T ASME* 138(8):1–14
16. Nakayama K, Arai M, Kanda T (1998) Machining characteristics of hard materials. *Ann CIRP* 37(1):89–92
17. Yang Y, Li J (2010) Study on mechanism of chip formation during high-speed milling of alloy cast iron. *J Adv Manuf Technol* 46(1–4):1655–1669
18. Zhou A, Deng F (2001) Experimental study on the heat treatment process for Cr12MoV steel. *Die Mould Ind* 000(9):55–57
19. Wang LJ, Miao B, Meng XX (2005) Analysis on the hardness and metallographic structure of Cr12MoV steel under different heat treatment. *Die Mould Ind* 9:52–56
20. Liu Z, Wan Y, Zhou J (2006) Tool materials for high speed machining and their fabrication technologies. *Mater Mech Eng* 30(5):1–4
21. Schulz H, Abele E, Sahn A (2001) Material aspects of chip formation in HSC machining. *CIRP Ann-Manuf Technol* 50(1):45–48
22. Yang Q, Wu Liu YD (2016) Characteristics of serrated chip formation in high-speed machining of metallic materials. *J Adv Manuf Technol* 86(5–8):1201–1206
23. Vyas A, Shaw MC (1999) Mechanics of saw-tooth chip formation in metal cutting. *J Manuf Sci E-T ASME* 121(2):163–172
24. Barry J, Byrne G (2002) The mechanisms of chip formation in machining hardened steels. *J Manuf Sci Eng* 124(3):528–535
25. EI-Wardany T, Kishawy HA, EI-bestawi MA (2000) Surface integrity of die material in high speed hard machining. Part 1: micrographical analysis. *J Manuf Sci E-T ASME* 122 (4): 620–631.
26. Poulachon GR, Moisan AL, Jawahir IS (2007) Evaluation of chip morphology in hard turning using constitutive models and material property data. *J Manuf Sci E-T ASME* 129(1):41–47